Forming Covalent Crosslinks between Polymer# Grafted Nanoparticles as a Route to Highly Filled and Mechanically Robust Nanocomposites

Forming Covalent Crosslinks between Polymer Grafted Nanoparticles as a Route to Highly Filled and Mechanically Robust Nanocomposites

*Joshua M. Kubiak and Robert J. Macfarlane**

J. M. Kubiak, Prof. R. J. Macfarlane
77 Massachusetts Avenue, Cambridge, MA, 02139, USA.
E-mail: rmacfarl@mit.edu

Keywords: composite materials, crosslinking, processing, polymeric materials, nanoparticles

Filler aggregation in polymer matrix nanocomposites leads to inhomogeneity in particle distribution and deterioration of mechanical properties. The use of polymer grafted nanoparticles (PGNPs) with polymers directly attached to the particle surfaces precludes aggregation of the filler. However, solids composed of PGNPs are mechanically weak unless the grafted chains are long enough to form entanglements between particles, and requiring long grafts limits the achievable filler density of the nanocomposite. In this work, long, entangled grafts are replaced with short reactive polymers that form covalent crosslinks between particles. Crosslinkable PGNPs, referred to as XNPs, can be easily processed from solution and subsequently cured to yield a highly filled yet mechanically robust composite. In this specific instance, silica nanoparticles are grafted with poly(glycidyl methacrylate), cast into films, and crosslinked with multifunctional amines at elevated temperatures. Indentation and scratch experiments show significant enhancement of hardness, modulus, and scratch resistance compared to non-crosslinked PGNPs and to crosslinked polymer films without nanoparticle reinforcement. Loadings of up to 57 wt% are achieved while yielding uniform films that deform locally in a predominantly elastic manner. XNPs therefore potentially allow for the formulation of robust nanocomposites with a high level of functionality imparted by the selected filler particles.

1. Introduction

Composite materials are commonly used when an application requires a combination of properties that is not obtainable from any single material. For example, car tires benefit from the elasticity of rubber with added durability and strength from carbon black filler,[1] high performance brake rotors combine the strength and low mass of carbon fiber with the heat resistance of ceramics,[2] and machine tools are made from abrasion resistant tungsten carbide and a tough cobalt metal matrix.[3] Owing to their low cost, low density, and ease of processing, polymers are often used as a matrix phase, with a fibrous or particulate filler added to provide mechanical reinforcement or add a specific function (e.g. electrical,[4,5] thermal,[6] optical,[7] or magnetic[8] properties).[9] Particulate fillers of a variety of compositions can be incorporated into thermosets or thermoplastics, and reducing the size of the filler particles to the nanometer scale often leads to further enhancement of mechanical properties or the development of emergent properties.[10–14]

While technologically useful,[15] polymer matrix nanocomposites are often limited in composition due to filler particle aggregation. At loadings greater than a few weight percent, particles cluster together to minimize unfavorable surface interactions between the filler particles and the surrounding matrix, resulting in an inhomogeneous nanocomposite.[16–18] This driving force for aggregation can be minimized by using compatibilizing surface ligands which reduce the chemical dissimilarity between filler and matrix,[19–21] or by synthesizing the nanoparticles in situ with sol-gel processing methods wherein the filler particles are dispersed in matrix precursors.[22–25] Nevertheless, even with these different synthesis and processing methods, the formation of aggregates can seldom be completely suppressed. One promising route to circumvent the aggregation of filler within the polymer matrix is to graft polymer chains directly to the surface of the particles, creating polymer-grafted nanoparticles (PGNPs).[26] Filler dispersion can be greatly improved using PGNPs when the grafted chains

match the composition of the free polymer chains of the matrix, or when the grafted chains and the polymer matrix have a negative interaction parameter.[27–30] PGNPs have been used to control the dielectric,[31,32] optical,[33,34] thermal,[35–37] magnetic,[27] and mechanical[30,38–40] properties of nanocomposites.[41] While the appropriate choice of particle-bound polymers can almost completely suppress aggregation of particles within the matrix,[29,42] the highest particle loadings are achieved when PGNPs with relatively short polymer grafts are used neat, without any additional free polymer. However, neat PGNP solids with short grafts are relatively soft and weak, as these short polymers are incapable of forming interchain entanglements between neighboring particles. Longer polymer grafts improve these limitations in mechanical properties, but also dilute the amount of core filler particles in the matrix, diminishing any functionality that the filler provides.[39,42,43] There is therefore a gap in the development of highly filled polymer matrix nanocomposites that are also mechanically robust. Here, we establish a new polymer composite synthesis method to address this challenge by creating PGNPs bearing short polymer grafts containing covalently crosslinkable chemical moieties. These crosslinkable PGNPs, hereafter referred to as XNPs, consist of silica nanoparticles (SiO_2 NPs) grafted with poly(glycidyl methacrylate) (PGMA) (**Figure 1**).[44–47] Each residue of PGMA contains an epoxide ring which can be reacted with a multifunctional amine to yield interparticle crosslinks. By replacing entanglements with covalent crosslinks between particles, we demonstrate that a mechanically robust nanocomposite solid can be obtained while maintaining a high density of filler particles, well beyond what has been achieved with previous PGNP composites.

2. Synthesis of XNPs

Uniform SiO_2 NPs were prepared using the Stöber method[48,49] and functionalized with bromoisobutyrate-bearing silanes[50] to allow PGMA chains to be grafted from the NPs via Surface Initiated Atom Transfer Racial Polymerization (SI-ATRP),[47,51,52] resulting in polymer

brushes with high grafting density and low polymer dispersity. The SiO_2 NPs were characterized by transmission election microscopy (TEM), the molecular weight distribution of the grafted chains was characterized by gel permeation chromatography (GPC), and the surface grafting density was determined using thermogravimetric analysis (TGA). A range of core particle sizes were examined to demonstrate the generality of this method for producing composites, and the length of the grafted chains was varied to probe the limit of filler particle density that could be achieved. The procedure for this XNP synthesis is shown in **Figure 1**, and **Table 1** details all of the materials prepared for this study.

3. Preparation and Curing of XNP Films

To prepare XNP solids for mechanical testing, films were made by drop casting solutions of XNPs with or without added diaminodiphenyl sulfone (DDS) curing agent onto silicon wafer pieces and allowing the films to slowly dry in a solvated atmosphere. Cast films were then subjected to one of two treatments: drying at 50 °C for 16 hours under vacuum or curing at 175 °C for 6 hours under vacuum. At elevated temperatures, the primary amines of DDS nucleophilically attack the pendant epoxide rings of PGMA (Figure 1), resulting in interchain and intrachain crosslinking.[53] DDS is not a significantly active curing agent below 100 °C, so the dried samples were used as non-crosslinked controls ("dried control"). Samples subjected to the curing treatment without any DDS were also prepared for comparison to the crosslinked films; they will hereafter be referred to as "annealed control" samples.

Attenuated total reflectance Fourier transform IR spectroscopy was used to confirm the reaction between grafted PGMA chains and DDS when thermally cured **(Figure S1)**.[54] For dried control samples and annealed control samples, no reaction of the epoxide ring was observed. The XNP strategy enabled the formation of crack-free, transparent films (**Figure S2**) with silica loadings of up to 57 wt% (**Figure 2**), an exceptionally high filler loading that cannot be easily

achieved by other processing methods without particle aggregation. As a demonstration of this limitation of other traditional composite processing methods, a film was cast from an equivalent solution blend of free PGMA and SiO_2 NPs and compared to an XNP film (Figure 2, d). The blend film was inhomogeneous, optically opaque, and not suitable for characterization by nanoindentation while the XNP film was uniform and transparent. Even with compatibilizing ligands, high energy mixing, or sol-gel processing methodologies, uniformly distributing nanoscale filler particles is difficult. Previous work has demonstrated the use of reactive surface-functionalizing groups (often called coupling agents) that allow for covalent bonding of matrix polymer to the filler particles resulting in improved mechanical properties and functionality.[55–61] However, these methods also suffer from particle clustering, whereas the proposed method ensures that a uniform, continuous layer of polymer is present between each inorganic core as shown in TEM images of XNP materials cast from dilute solution and heated in the presence of DDS **(Figure S3)**. Additionally, no evidence of polymer degradation is observed, and TGA of XNPs prior to processing into a film also indicated that the PGMA grafts were stable during the curing conditions **(Figure S4)**. Therefore, any changes in properties after curing are attributed to the formation of covalent crosslinks rather than thermal degradation or a loss of organic content.

4. Mechanical Testing of XNP Films

The introduction of covalent bonds between particles should increase the amount of energy required to displace particles from their neighbors, resulting in an increased resistance to deformation as measured by hardness. Crosslinked XNP materials would also be expected to have a higher elastic modulus than non-crosslinked XNP films, since the covalent interparticle bonds are strained during reversible deformation. To demonstrate these effects of crosslinking on the mechanical properties of XNP solids, nanoindentation was performed on the crosslinked and control films; hardness and reduced modulus were determined by Oliver-Pharr[62] analysis

of indentation experiments using a rate-jump[63–65] method and plastic contact modification.[64] Furthermore, as a result of the high inorganic content, the coherence of the interface between filler and matrix,[66,67] and the strengthened interparticle interactions, XNP films would be expected to be more resistant to physical damage, which was examined by scratch testing.

4.1 Indentation of XNP Films

To create the most robust nanocomposite possible, the optimal proportion of DDS crosslinker was determined by measuring hardness and reduced modulus as a function of the equivalents of crosslinker used. It was hypothesized that adding excess DDS would be detrimental to film mechanical properties, as the added DDS would dilute the inorganic content of the composite. Additionally, because the polymer chains in the particle brush are densely packed, it could be hypothesized that neighboring particles only interact through a thin outer corona of the grafted chains, meaning that 100% equivalents of DDS with all monomer residues is unnecessary. Here, equivalents are defined as the ratio of DDS amine functional groups (two per DDS molecule) to epoxide rings (one per GMA monomer residue). It is worth noting that the hydroxyl groups of the opened epoxide rings as well as the secondary amines generated as a result of the DDS-epoxide reaction can also react with additional epoxides, but do so at a much slower rate. Therefore, the majority of covalent bonds formed between PGMA XNPs should result from DDS-driven ring opening. Above 25% equivalents for 49nm SiO_2-*g*-23kDa PGMA, the measured hardness and modulus of the material reached plateau values of approximately 425 MPa and 8 GPa, respectively, consistent with the hypothesis above. Moreover, films with greater than 25% equivalents of DDS tended to exhibit greater amounts of undesirable roughness (**Figure S5** and **S6**). Based on these results, 25% equivalents of DDS were used for the remainder of the experiments in this study.

For a given core size, decreasing the length of the grafted chains increases the concentration of the much harder and stiffer SiO_2 particles. As a result, XNPs with shorter polymer grafts exhibit increased hardness and modulus after crosslinking (**Figure 3** and **S7**). For all core sizes, both hardness and reduced modulus increased as graft molecular weight was decreased, and significantly higher hardness values were measured for crosslinked films compared to annealed or dried control samples. The improved hardness of crosslinked XNPs attests to the successful formation of covalent interparticle bonds during curing which increases the strength of interparticle interactions, yielding a stronger composite.

The reduced modulus of crosslinked XNPs was also significantly greater than the dried control materials, indicating a greater resistance to elastic deformation. However, the measured modulus values for control samples annealed without DDS were similar to those for the crosslinked samples; this observation is attributed to the compressive nature of the indentation experiments. During the test, XNPs are compacted, pushing densely packed polymer grafts into each other.[68,69] As the load is released, the material's elastic recovery is largely caused by the steric repulsion between the compressed polymer chains, regardless of whether or not crosslinks exist between particles.

In addition, both reduced modulus and hardness were greater for all annealed control materials compared to the corresponding dried controls, even though neither of these sample sets were crosslinked. The augmented properties of annealed control samples are attributed to the lack of unreacted DDS (which acts as a diluent and plasticizer),[70] as well as to film densification during thermal treatment above the glass transition temperature (T_g) of PGMA (~80 °C for linear PGMA).**[71]** In fact, for XNPs with the shortest polymer grafts (and therefore the highest filler loadings) it was not possible to obtain modulus and hardness values for control samples because the films cracked during drying or annealing. This observation supports the above

premise that DDS acts as a plasticizer and that heating above the T_g of PGMA may allow the polymer chains to rearrange and relieve internal stresses to avoid film cracking during processing.

It is also emphasized that all crosslinked XNP materials had hardness and reduced modulus values greater than those of free PGMA crosslinked with 25% equivalents of DDS. The 116nm SiO_2-*g*-32kDa PGMA material exhibited the largest improvements over the corresponding polymer-only materials—67% and 111% for reduced modulus and hardness, respectively. This improvement in mechanical properties is drastically different from past studies of films of neat, non-crosslinkable PGNPs with long polymer chains, which exhibited properties equivalent to those of the bulk polymer at best.[39,42] Therefore, the use of covalent crosslinks provides significant advancement in the preparation of mechanically robust composite films compared to previous synthesis methods.

4.2 Scratch Testing of XNP Materials

Composites with weak interactions between particles should be more easily scratched than composites with strong, covalent interactions, and less plastic deformation and greater elasticity would also be predicted for samples connected via covalent bonds. To test these hypotheses, scratch testing was performed on both crosslinked and annealed control samples (representative surface profile traces are shown in **Figure S8**. Generally, scratches made in the non-crosslinked films were deeper, and the post-scratch traces showed little elastic recovery and significant evidence of the pileup of displaced particles at the end of the scratch. In contrast, scratches in the crosslinked films were shallower, and the post-scratch traces indicated that most of the deformation was elastic and quickly recovered with no evidence of pile-up. Changes in the deformation behavior of the material as a result of crosslinking were directly observed by Helium Ion Microscopy (HIM) of the scratches. For a representative sample from each core-

size, the non-crosslinked samples were observed to deform plastically (**Figure 4**), with deep trenches and fringes of displaced particles, while images of crosslinked materials showed very little permanent deformation or particle displacement. The differences between the scratch and post-scratch traces, relative to the pre-scratch traces, are summarized for all tested samples as a fractional recovery value in **Figure 5**. In all cases, there was much greater permanent, plastic deformation in the non-crosslinked samples. Interestingly, XNP materials exhibited remarkable local elasticity even for shorter polymer grafts, which is impressive for materials with nearly 60 wt% of SiO_2 filler. The elastic recovery of crosslinked films is attributed to the relative stiffness difference of silica and crosslinked PGMA; when under stress, deformation is localized to the continuous and elastic polymer layer between each silica particle, allowing the composite as a whole to quickly recover. Thus, the formation of crosslinks between XNPs yields a locally elastic and damage-resistant highly filled composite material.

4.3 Mechanical Testing Summary

The mechanical testing data from all samples can be reduced by viewing hardness and reduced modulus as functions of filler content, a product of particle size, grafting density, and graft length (**Figure 6**). A lower-bound rule of mixtures estimate for combinations of PGMA crosslinked with 25% equivalents of DDS and fused silica is plotted for comparison; the rule assumes equal stress in both constituents of the composite. Hardness and modulus are positively correlated with filler content, showing that the filler particles do have a reinforcing effect. Measured hardness values for cured XNP films are approximately equal to or slightly exceed the prediction of the rule of mixtures, with deviation above the estimate being the greatest at the highest filler loadings explored in this study. The additional enhancement is attributed to the diminishing size of the polymer interlayer between particles as filler loading is increased. Polymer chains in the interlayer are highly constrained by both the particle surfaces and the covalent crosslinks introduced by DDS, and, as a result, the grafted chains behave more rigidly

than free chains in the corresponding bulk polymer. Additionally, the reduced moduli of the XNP materials are well-predicted by the lower bound for the rule of mixtures, and agreement with the rule indicates that there is a cohesive interface between the polymer matrix and filler particles, as would be expected given that the core particles are covalently bonded to the polymer grafts.

5. Conclusion

The crosslinking of epoxy based XNPs with a variety of polymer lengths and core sizes enables remarkably high filler loadings, which lead to significantly enhanced stiffness, hardness, and damage resistance. The demonstrated method of producing particle-filled materials by crosslinking PGNPs with short, reactive polymer grafts enables the fabrication of nanocomposites with high filler densities that cannot be achieved using more traditional techniques. Simultaneously, and in sharp contrast to non-crosslinked PGNPs previously reported, the mechanical properties of the composite were enhanced with increasing filler density. In many applications of polymer matrix nanocomposites, the desired functional characteristics improve with increased filler loadings, but the composition is ultimately limited by aggregation. The XNP method for obtaining composites with robust mechanical properties allows for greater functionality to be imparted to a composite by the incorporation of a large degree of inorganic content. In principle, this should allow for a range of beneficial composite materials through judicious selection of filler particle composition, for instance alumina for enhanced thermal conductivity, titania to increase refractive index, or iron for electromagnetic shielding. The use of crosslinkable polymer grafted nanoparticles to create highly filled composite solids is therefore an optimal strategy for fabricating designer composite materials with specific and desirable property combinations.

6. Experimental Section

Glycidyl methacrylate was filtered through neutral alumina prior to use to remove inhibitor. All solvents and other reagents were purchased from Sigma or Fisher and used as received. Silicon wafer pieces were cleaned with acetone, isopropanol, and water and dried under nitrogen flow prior to use. A stock solution of Copper (II) Bromide ($CuBr_2$) in dimethylformamide (DMF) (20 mg/mL) was prepared for the polymerization reactions.

Tetherable Initiator Synthesis:

The tetherable initiator was prepared in two steps as previously reported.[50] First, α-bromoisobutyryl bromide and 5-hexen-1-ol were combined in an esterification reaction to yield 1-(2-bromo-2-methyl)propionyloxy-5-hexene (BPH). Next, BPH was combined with triethoxysilane by hydrosilation to yield (2-Bromo-2-methyl)propionyloxyhexyltriethoxysilane (BHE), which was stored in a dark cabinet until use. See Supporting Information for synthetic details.

Silica Nanoparticle Synthesis: Silica nanoparticles were prepared using the Stöber method.[48,49] In a typical reaction to produce approximately 100 nm diameter particles, deionized water (10.3 mL), ammonia solution (28 wt%, 67.6 mL), and 200 proof ethanol (884 mL) were combined in a 2L flask with a magnetic stir bar. The solution was heated to 40 °C using a thermocouple controlled heating mantle. Once the temperature was stable, tetraethoxyorthosilicate (TEOS) (38 mL) was added quickly while stirring. The reaction was allowed to proceed for at least three hours. Then, while maintaining a temperature of 40 °C, approx. 4 g of BHE was added incrementally over 24 hours. The resulting particles were purified by three cycles of centrifugation and redispersion in ethanol followed by three cycles of centrifugation and redispersion in anisole. Particles were stored as a stock solution in anisole and redispersed in DMF for use in the polymerization reactions. TEM images of all three sizes of NPs used in this study are shown in **Figure S9**.

SI-ATRP: To prepare a typical particle brush, SiO_2-BHE stock solution (5 g, 20 uM), ethyl α-bromoisobutyrate (18 uL, 6 uM), GMA (6.9 mL, 52 mM), $CuBr_2$ (8.7 mg, 39 uM), and bypyridine (67 mg, 0.43 mM) were dissolved in anhydrous DMF (9 mL) in a 50 mL Schlenk flask equipped with a rare-earth magnetic stir bar. The solution was degassed by four cycles of freeze-pump-thaw. The flask was back-filled with nitrogen gas, and opened under nitrogen flow. CuBr (23 mg, 0.16 mM) was added on top of the frozen solution, and the flask was resealed. While frozen, the flask was evacuated and re-filled with nitrogen gas three times. The reaction mixture was then thawed, and the polymerization was allowed to proceed at room temperature while tracking progress with ^{1}H NMR. At the desired monomer conversion, the flask was opened to air, oxygenated THF was added, and the solution was filtered through neutral alumina. The grafted particles were purified by three cycles of centrifugation and redispersion in THF followed by precipitation into hexanes to yield a slightly blue powder. The supernatant from the first centrifugation was collected and precipitated into cold ether. The precipitant was dissolved in THF and precipitated again in ether followed by dissolution and precipitation in hexanes to yield free polymer as a white powder. Both particles and free polymer were dried under vacuum at room temperature, and stored in a freezer until used.

FTIR: Attenuated total reflectance (ATR) FTIR was performed on a Thermo Fisher FTIR6700 spectrophotometer with a Thermo Fisher Continuum Infrared microscope using a hemispherical Germanium crystal. Spectra were subjected to automatic background subtraction and ATR correction.

TGA: TGA was performed on a TA instruments Discovery using high-temperature platinum pans. Measurements were performed under nitrogen gas with a 15 min hold at 150 °C to remove residual solvents before heating to 800 °C at 15 °C/min.

GPC: GPC was performed on an Agilent 1260 Infinity II system with a multi-detector suite using two sequential Agilent ResiPore columns and 0.1 µm filtered tetrahydrofuran (THF) as the eluent at 40 °C and a flow rate of 1 mL/min. Absolute molecular weights were determined using refractive index (RI) and light scattering (90°) detectors (dn/dc = 0.093 mL/g).

TEM: TEM was performed on an FEI Tecnai (G2 Spirit TWIN) digital TEM at an accelerating voltage of 120 kV. Samples were prepared by drop casting from 2 mg/mL solutions in 2-butanone/2-pentanone onto carbon coated copper grids and drying in air. Grids were then heated for 6 hours at 175 °C in a vacuum oven.

Film Casting: Films were cast from 40 mg/mL solutions of XNPs and DDS in mixtures of 2-butanone and 2-pentanone. The solvent ranged from 3:1 to 1:1 by volume of 2-pentanone/2-butanone. Longer graft lengths typically required a greater proportion of 2-butanone to dissolve, while too much 2-butanone lead to more significant 'fairy rings' or film cracking. Approximately 80 uL was deposited onto each 1 cm x 1 cm wafer piece inside a glass desiccator. Additional solvent was added to the desiccator to saturate the atmosphere with solvent vapor, and the lid was placed onto the desiccator with a small gap to allow for solvent evaporation. Films prepared from XNPs with 116 nm cores tended to exhibit surface wrinkling, so care was taken to perform mechanical measurements in regions that were flat. Films were then heated in a vacuum oven at either 50 °C or 175 °C. Preliminary experiments showed that 6 hrs was sufficient for significant crosslinking (**Figure S10**).

Nanoindentation: Both indentation and scratch experiments were performed on a Hysitron Triboindenter. A Berkovich tip and 1-D DMA transducer were used for indentation, and the instrument was operated in load-control with 100 µN/s loading and unloading rates to a peak

load of 7500 µN with a 90 second constant-load hold. For each sample, 25 indentations were made. A maximum depth of ~1500 nm was reached during these experiments, and film thicknesses were measured by stylus profilometry to be > 20 µm. Representative indentation depth-load curves are displayed in **Figure S11**. Data were analyzed in MATLAB using the rate-jump method between the constant-load and unloading steps to minimize viscoelastic effects. As a result of significant deformation during indentation, a plastic contact assumption was found to be appropriate for all samples. Since the indenter tip is much stiffer than the composite films, the reduced modulus is approximately equal to the plane-strain modulus of the material. For scratch testing, a 1 µm conospherical tip and 2-D transducer were used. The initial surface profile was traced with minimal normal force before applying 750 µN and creating a 10 µm long scratch at a lateral displacement rate of 400 nm/s. After removing the load, the profile of the scratch was again traced with minimal normal force. The scratch recovery for each sample was calculated using MATLAB. The initial surface profile was subtracted from both the during-scratch and after-scratch profiles to account for surface roughness and slant. Recovery was determined from the center area (free of pile-up or dig-in) of each scratch as the difference between the scratch depth and recovery depth normalized by the scratch depth. Ten scratches were made in each sample.

Profilometry: Film thickness was measured on a Bruker DXT stylus profilometer.

He Ion Imaging: HIM was performed on a Zeiss Orion Plus NanoFab microscope with an accelerating voltage of 32.5 kV. Films were coated in a thin layer (~2 nm) of gold prior to imaging.

Supporting Information
Supporting Information is available from the Wiley Online Library or from the author.

Acknowledgements

Joshua Kubiak was supported by the Department of Defense (DoD) through the National Defense Science & Engineering Graduate Fellowship (NDSEG) Program. This work was supported by an NSF CAREER Grant, award number CHE-1653289 and made use of the MRSEC Shared Experimental Facilities at MIT, supported by the NSF under Award DMR 14-19807. This work also made us of the NanoMechanical Technology Laboratory in the Department of Materials Science and Engineering at MIT. Thanks are given to Leonardo Zornberg, Mathew Suazo, and Sara Wilson for aiding in sample preparation prior to experimental measurements.

Received: ((will be filled in by the editorial staff))
Revised: ((will be filled in by the editorial staff))
Published online: ((will be filled in by the editorial staff))

References

[1] D. J. Kohls, G. Beaucage, *Curr. Opin. Solid State Mater. Sci.* **2002**, *6*, 183.

[2] M. Krupka, A. Kienzle, *SAE Int.*, **2000**, DOI 10.4271/2000-01-2761.

[3] K. Jia, T. E. Fischer, B. Gallois, *Nanostructured Mater.* **1998**, *10*, 875.

[4] W. Liu, S. W. Lee, D. Lin, F. Shi, S. Wang, A. D. Sendek, Y. Cui, *Nat. Energy* **2017**, *2*, 17035.

[5] D. Lin, W. Liu, Y. Liu, H. R. Lee, P.-C. Hsu, K. Liu, Y. Cui, *Nano Lett.* **2016**, *16*, 459.

[6] A. Tessema, D. Zhao, J. Moll, S. Xu, R. Yang, C. Li, S. K. Kumar, A. Kidane, *Polym. Test.* **2017**, *57*, 101.

[7] C. C. D. Wang, W. C. H. Choy, C. Duan, D. D. S. Fung, W. E. I. Sha, F.-X. Xie, F. Huang, Y. Cao, *J Mater Chem* **2012**, *22*, 1206.

[8] M. Jalali, S. Dauterstedt, A. Michaud, R. Wuthrich, *Compos. Part B Eng.* **2011**, *42*, 1420.

[9] R. Wang, S. Zheng, Y. Zheng, *Polymer matrix composites and technology*,Woodhead, Cambridge, England **2011**.

[10] L. Sun, R. F. Gibson, F. Gordaninejad, J. Suhr, *Compos. Sci. Technol.* **2009**, *69*, 2392.

[11] Kilwon Cho, JaeHo Yang, Chan Eon Park, *Polymer* **1998**, *39*, 3073.

[12] M. Quaresimin, K. Schulte, M. Zappalorto, S. Chandrasekaran, *Compos. Sci. Technol.* **2016**, *123*, 187.

[13] S. C. Tjong, *Mater. Sci. Eng. R Rep.* **2006**, *53*, 73.

[14] G. A. Williams, R. Ishige, O. R. Cromwell, J. Chung, A. Takahara, Z. Guan, *Adv. Mater.* **2015**, *27*, 3934.

[15] S. K. Kumar, B. C. Benicewicz, R. A. Vaia, K. I. Winey, *Macromolecules* **2017**, *50*, 714.

[16] S. Kango, S. Kalia, A. Celli, J. Njuguna, Y. Habibi, R. Kumar, *Prog. Polym. Sci.* **2013**, *38*, 1232.

[17] G. Kickelbick, *Prog. Polym. Sci.* **2003**, *28*, 83.

[18] C. Cochrane, V. Koncar, M. Lewandowski, C. Dufour, *Sensors* **2007**, *7*, 473.

[19] P. Reichert, H. Nitz, S. Klinke, R. Brandsch, R. Thomann, R. Mülhaupt, *Macromol. Mater. Eng.* **2000**, *275*, 8.

[20] P. Kim, S. C. Jones, P. J. Hotchkiss, J. N. Haddock, B. Kippelen, S. R. Marder, J. W. Perry, *Adv. Mater.* **2007**, *19*, 1001.

[21] L. Vaisman, G. Marom, H. D. Wagner, *Adv. Funct. Mater.* **2006**, *16*, 357.

[22] C.-H. Hung, W.-T. Whang, *J. Mater. Chem.* **2005**, *15*, 267.

[23] B. M. Novak, *Adv. Mater.* **1993**, *5*, 422.

[24] B. B. Johnsen, A. J. Kinloch, R. D. Mohammed, A. C. Taylor, S. Sprenger, *Polymer* **2007**, *48*, 530.

[25] H. Zhang, Z. Zhang, K. Friedrich, C. Eger, *Acta Mater.* **2006**, *54*, 1833.

[26] C. M. Hui, J. Pietrasik, M. Schmitt, C. Mahoney, J. Choi, M. R. Bockstaller, K. Matyjaszewski, *Chem. Mater.* **2014**, *26*, 745.

[27] Y. Jiao, P. Akcora, *Macromolecules* **2012**, *45*, 3463.

[28] C. Chevigny, F. Dalmas, E. Di Cola, D. Gigmes, D. Bertin, F. Boué, J. Jestin, *Macromolecules* **2011**, *44*, 122.

[29] D. Sunday, J. Ilavsky, D. L. Green, *Macromolecules* **2012**, *45*, 4007.

[30] J. M. Kubiak, J. Yan, J. Pietrasik, K. Matyjaszewski, *Polymer* **2017**, *117*, 48.

[31] C. A. Grabowski, H. Koerner, J. S. Meth, A. Dang, C. M. Hui, K. Matyjaszewski, M. R. Bockstaller, M. F. Durstock, R. A. Vaia, *ACS Appl. Mater. Interfaces* **2014**, *6*, 21500.

[32] S. Virtanen, T. M. Krentz, J. K. Nelson, L. S. Schadler, M. Bell, B. Benicewicz, H. Hillborg, Su Zhao, *IEEE Trans. Dielectr. Electr. Insul.* **2014**, *21*, 563.

[33] P. Tao, A. Viswanath, L. S. Schadler, B. C. Benicewicz, R. W. Siegel, *ACS Appl. Mater. Interfaces* **2011**, *3*, 3638.

[34] Y. Li, P. Tao, A. Viswanath, B. C. Benicewicz, L. S. Schadler, *Langmuir* **2013**, *29*, 1211.

[35] Y. Huang, Y. Zheng, A. Sarkar, Y. Xu, M. Stefik, B. C. Benicewicz, *Macromolecules* **2017**, *50*, 4742.

[36] Y. Cang, A. N. Reuss, J. Lee, J. Yan, J. Zhang, E. Alonso-Redondo, R. Sainidou, P. Rembert, K. Matyjaszewski, M. R. Bockstaller, G. Fytas, *Macromolecules* **2017**, *50*, 8658.

[37] C. Mahoney, C. M. Hui, S. Majumdar, Z. Wang, J. A. Malen, M. N. Tchoul, K. Matyjaszewski, M. R. Bockstaller, *Polymer* **2016**, *93*, 72.

[38] M. Giovino, J. Pribyl, B. Benicewicz, R. Bucinell, L. Schadler, *Nanocomposites* **2018**, *4*, 244.

[39] J. Choi, C. M. Hui, J. Pietrasik, H. Dong, K. Matyjaszewski, M. R. Bockstaller, *Soft Matter* **2012**, *8*, 4072.

[40] E. Alonso-Redondo, M. Schmitt, Z. Urbach, C. M. Hui, R. Sainidou, P. Rembert, K. Matyjaszewski, M. R. Bockstaller, G. Fytas, *Nat. Commun.* **2015**, *6*.

[41] S. K. Kumar, N. Jouault, B. Benicewicz, T. Neely, *Macromolecules* **2013**, *46*, 3199.

[42] J. Yan, T. Kristufek, M. Schmitt, Z. Wang, G. Xie, A. Dang, C. M. Hui, J. Pietrasik, M. R. Bockstaller, K. Matyjaszewski, *Macromolecules* **2015**, *48*, 8208.

[43] M. Schmitt, J. Choi, C. Min Hui, B. Chen, E. Korkmaz, J. Yan, S. Margel, O. Burak Ozdoganlar, K. Matyjaszewski, M. R. Bockstaller, *Soft Matter* **2016**, *12*, 3527.

[44] H. J. Zhou, M. Z. Rong, M. Q. Zhang, B. Lehmann, K. Friedrich, *Polym. J.* **2005**, *37*, 677.

[45] K. Jlassi, S. Chandran, M. Mičušik, M. Benna-Zayani, Y. Yagci, S. Thomas, M. M. Chehimi, *Eur. Polym. J.* **2015**, *72*, 89.

[46] P. Tao, A. Viswanath, Y. Li, R. W. Siegel, B. C. Benicewicz, L. S. Schadler, *Polymer* **2013**, *54*, 1639.

[47] M. Lillethorup, K. Shimizu, N. Plumeré, S. U. Pedersen, K. Daasbjerg, *Macromolecules* **2014**, *47*, 5081.

[48] Y. Huang, J. E. Pemberton, *Colloids Surf. Physicochem. Eng. Asp.* **2010**, *360*, 175.

[49] W. Stöber, A. Fink, E. Bohn, *J. Colloid Interface Sci.* **1968**, *26*, 62.

[50] K. Ohno, T. Morinaga, K. Koh, Y. Tsujii, T. Fukuda, *Macromolecules* **2005**, *38*, 2137.

[51] L. Yuan, X. Hua, Y. Wu, X. Pan, S. Liu, *Anal. Chem.* **2011**, *83*, 6800.

[52] S. Edmondson, W. T. S. Huck, *J. Mater. Chem.* **2004**, *14*, 730.

[53] J. C. Song, C. S. P. Sung, *Macromolecules* **1993**, *26*, 4818.

[54] W. A. Patterson, *Anal. Chem.* **1954**, *26*, 823.

[55] M. Z. Rong, M. Q. Zhang, W. H. Ruan, *Mater. Sci. Technol.* **2006**, *22*, 787.

[56] R. Y. Hong, H. P. Fu, Y. J. Zhang, L. Liu, J. Wang, H. Z. Li, Y. Zheng, *J. Appl. Polym. Sci.* **2007**, *105*, 2176.

[57] S. Mallakpour, A. Barati, *Prog. Org. Coat.* **2011**, *71*, 391.

[58] I. D. Sideridou, M. M. Karabela, *Dent. Mater.* **2009**, *25*, 1315.

[59] M. Sabzi, S. M. Mirabedini, J. Zohuriaan-Mehr, M. Atai, *Prog. Org. Coat.* **2009**, *65*, 222.

[60] S. M. Khaled, R. Sui, P. A. Charpentier, A. S. Rizkalla, *Langmuir* **2007**, *23*, 3988.

[61] M. Donnay, S. Tzavalas, E. Logakis, *Compos. Sci. Technol.* **2015**, *110*, 152.

[62] W. C. Oliver, G. M. Pharr, *J. Mater. Res.* **2004**, *19*, 3.

[63] A. H. W. Ngan, B. Tang, *J. Mater. Res.* **2009**, *24*, 853.

[64] N. Fujisawa, M. V. Swain, *J. Mater. Res.* **2006**, *21*, 708.

[65] B. Tang, A. H. W. Ngan, *J. Mater. Res.* **2003**, *18*, 1141.

[66] S.-Y. Fu, X.-Q. Feng, B. Lauke, Y.-W. Mai, *Compos. Part B Eng.* **2008**, *39*, 933.

[67] A. M. Pourrahimi, R. T. Olsson, M. S. Hedenqvist, *Adv. Mater.* **2018**, *30*, 1703624.

[68] D. C. Lin, E. K. Dimitriadis, F. Horkay, *Express Polym. Lett.* **2007**, *1*, 576.

[69] G. Kermouche, J. L. Loubet, J. M. Bergheau, *Mech. Mater.* **2008**, *40*, 271.

[70] A. Vazquez, D. Bentaleb, R. J. J. Williams, *J. Appl. Polym. Sci.* **1991**, *43*, 967.

[71] J. M. Jin, J. M. Lee, M. H. Ha, K. Lee, S. Choe, *Polymer* **2007**, *48*, 3107.

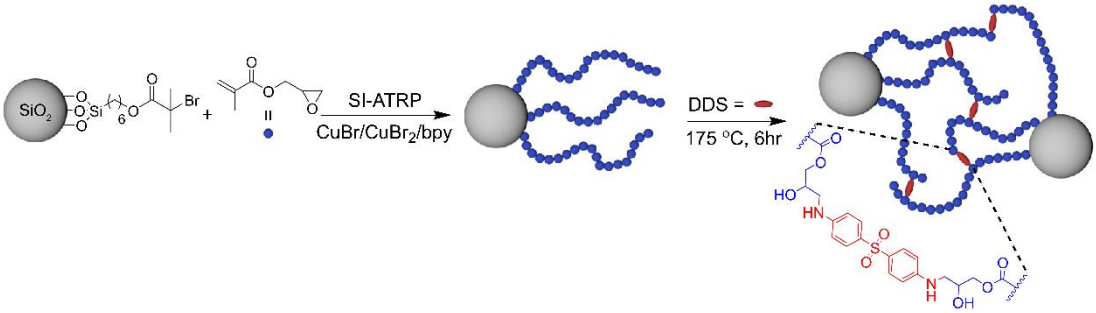

Figure 1. Synthesis of SiO_2-*g*-PGMA by surface initiated ATRP of glycidyl methacrylate from SiO_2 NPs and subsequent crosslinking by epoxide ring opening with DDS at elevated temperatures.

Table 1. Sample information for epoxy XNPs produced for this study.

Sample	SiO_2 Core Diameter [nm]	PGMA M_n [Da][a]	Grafting Density [chains/nm^2][b]	% Silica [wt%]
49nm SiO_2-*g*-15kDa PGMA	49 ± 10	14,600	0.41	55
49nm SiO_2-*g*-23kDa PGMA	49 ± 10	22,800	0.37	48
49nm SiO_2-*g*-28kDa PGMA	49 ± 10	27,500	0.39	43
49nm SiO_2-*g*-46kDa PGMA	49 ± 10	46,400	0.41	30
116nm SiO_2-*g*-32kDa PGMA	116 ± 10	31,800	0.37	61
116nm SiO_2-*g*-35kDa PGMA	116 ± 10	35,400	0.39	57
116nm SiO_2-*g*-39kDa PGMA	116 ± 10	38,500	0.47	52
116nm SiO_2-*g*-41kDa PGMA	116 ± 10	40,500	0.48	50
116nm SiO_2-*g*-65kDa PGMA	116 ± 10	64,900	0.29	51
116nm SiO_2-*g*-85kDa PGMA	116 ± 10	84,700	0.32	42
237nm SiO_2-*g*-76kDa PGMA	237 ± 9	76,200	0.42	55
237nm SiO_2-*g*-91kDa PGMA	237 ± 9	91,100	0.33	57
237nm SiO_2-*g*-135kDa PGMA	237 ± 9	135,000	0.27	53

[a)]Determined from simultaneously-synthesized free polymer produced in the SI-ATRP reaction; [b)]Silica density assumed as 2 g/cm^3

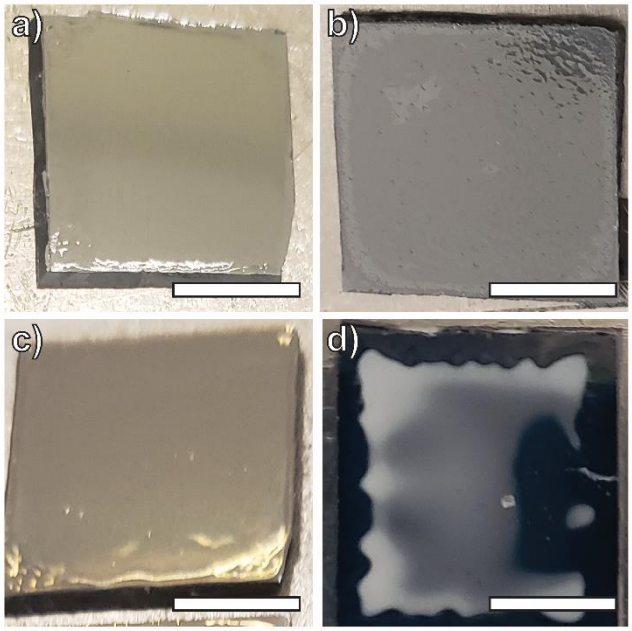

Figure 2. a) 49nm SiO_2-*g*-23kDa PGMA, b) 116nm SiO_2-*g*-35kDa PGMA, c) 237nm SiO_2-*g*-135kDa PGMA crosslinked XNP film images; d) equivalent solution blend of 116nm SiO_2 NPs and linear 35 kDa PGMA showing poor film quality. All scale bars are 5 mm.

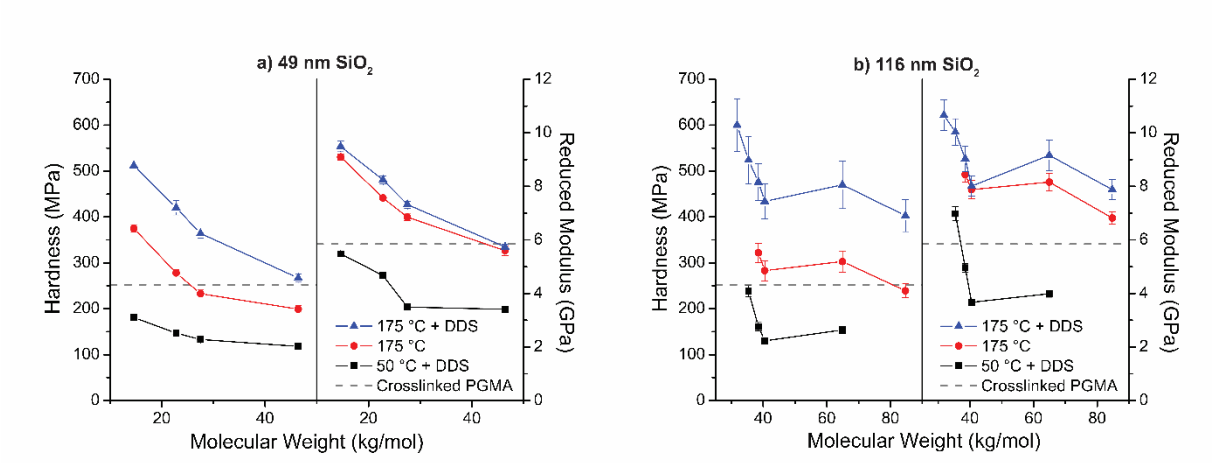

Figure 3. Hardness and reduced modulus as determined by nanoindentation for (a) 49 nm and (b) 116 nm core NPs of varying graft length. DDS crosslinked PGMA values (41 kDa) are plotted for comparison.

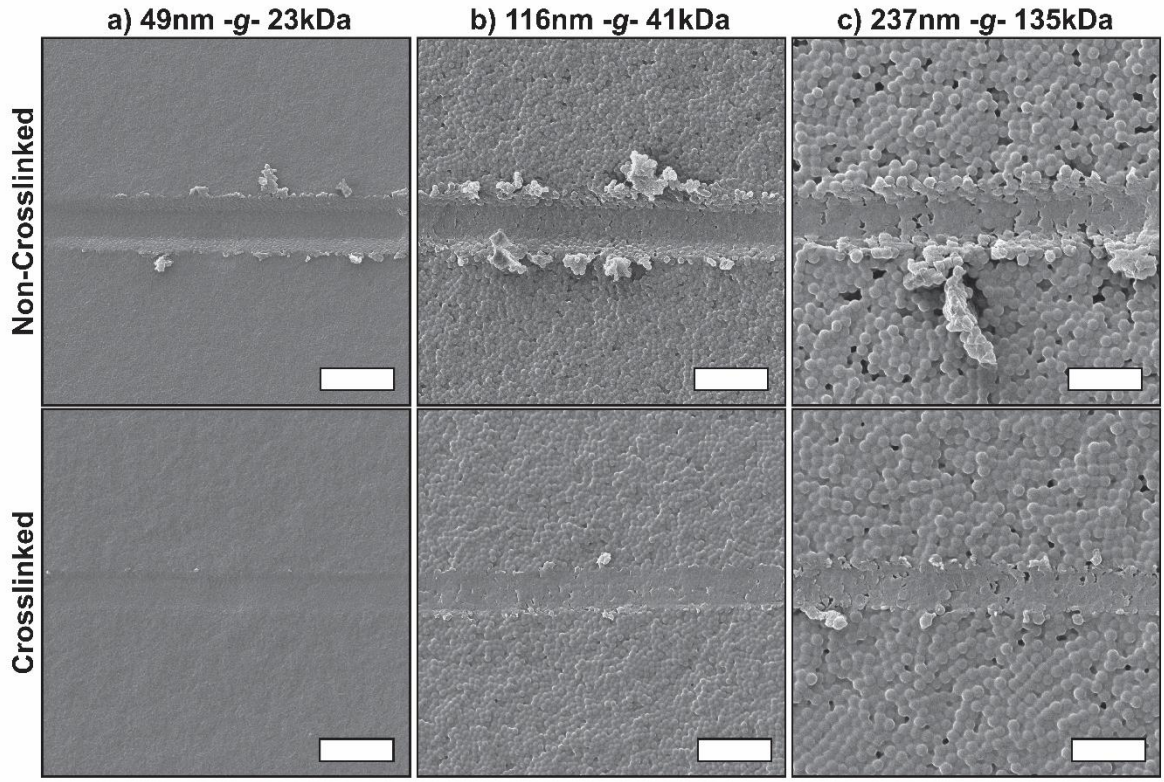

Figure 4. Helium ion microscopy images for non-crosslinked (top) and crosslinked (bottom) composites after scratch testing. (a) 49nm SiO_2-*g*-23kDa PGMA, (b) 116nm SiO_2-*g*-41kDa PGMA, and (c) 237nm SiO_2-*g*-135kDa PGMA all exhibit significant plastic deformation in non-crosslinked materials, compared with the predominantly elastic behavior observed in crosslinked materials. All scale bars are 1 µm.

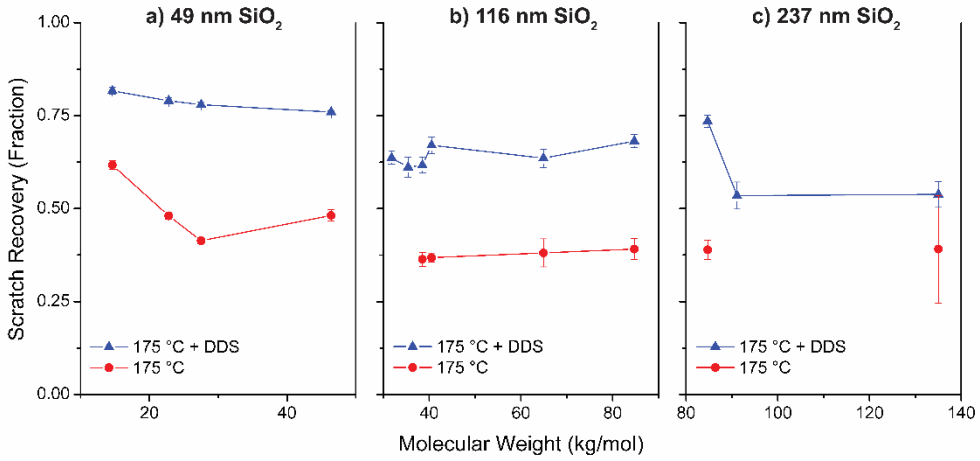

Figure 5. Scratch recovery for epoxy XNPs with (a) 49 nm, (b) 116 nm, and (c) 237 nm diameter cores and varying graft lengths showing significant improvements in damage resistance after crosslinking.

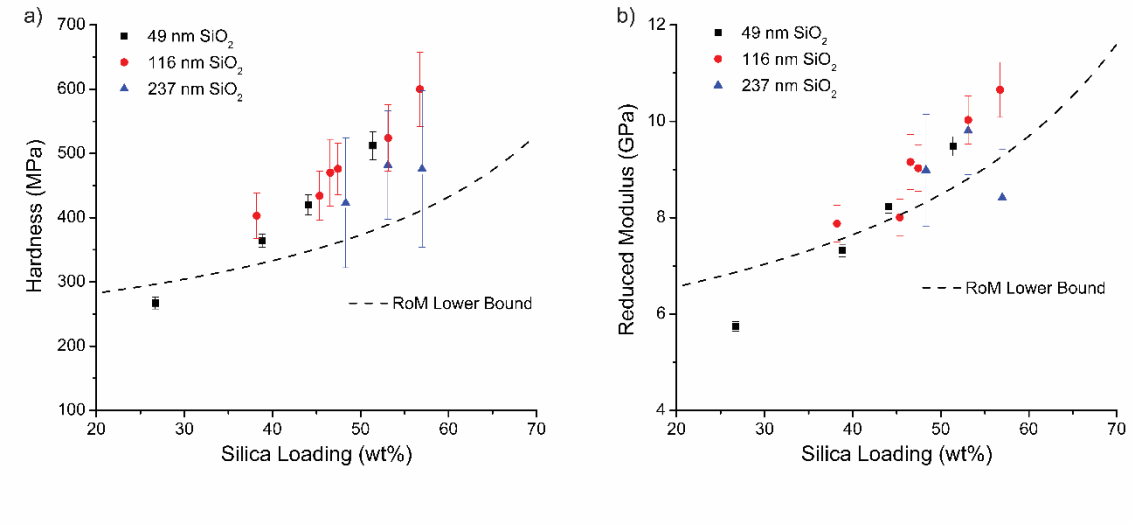

Figure 6. a) Hardness and (b) reduced modulus as determined by nanoindentation for all XNP core sizes as a function of silica loading. XNP properties are similar to those predicted by the lower bound of the rule of mixtures (RoM) between crosslinked PGMA and fused silica.